Journal of Radiation Research and Applied Sciences 18 (2025) 101203

Contents lists available at ScienceDirect

Journal of Radiation Research and Applied Sciences

journal homepage: www.journals.elsevier.com/journal-of-radiation-research-and-applied-sciences

Cell survival analysis of radiosensitization effects by gold nanoparticles for proton beam therapy

Raizulnasuha Ab Rashid [a,*], Noor Nabilah Talik Sisin [b], Khairunisak Abdul Razak [c], Moshi Geso [d], Hiroaki Akasaka [e], Ryohei Sasaki [e], Takahiro Tominaga [f], Hayato Miura [g], Masashi Nishi [g], Aml Aied Almutery [b,h], Wan Nordiana Rahman [b,i]

[a] Centre for Diagnostic Nuclear Imaging, Universiti Putra Malaysia, 43400, Serdang, Selangor, Malaysia
[b] Department of Applied Physics, Faculty of Science and Technology, Universiti Kebangsaan Malaysia, Bangi, Selangor, Malaysia
[c] School of Materials and Mineral Resources Engineering, Universiti Sains Malaysia, 14300, Penang, Malaysia
[d] School of Health and Biomedical Sciences, RMIT University, 3083, Victoria, Australia
[e] Graduate School of Medicine, Kobe University, 650-0017, Kobe, Japan
[f] Faculty of Health Sciences, Hiroshima International University, 739-2695, Hiroshima, Japan
[g] Hyogo Ion Beam Medical Centre (HIBMC), 679-5165, Hyogo, Japan
[h] Physics Department, Faculty of Science and Humanities in Ad-Dawadmi, Shaqra University, Shaqra, 11911, Saudi Arabia
[i] Nuclear Technology Research Centre, Faculty of Science and Technology, Universiti Kebangsaan Malaysia, 43600, UKM Bangi, Selangor, Malaysia

ARTICLE INFO

Keywords:
Gold nanoparticles
Proton beam therapy
Radiosensitization
Radiobiological model

ABSTRACT

Combining therapy and radiosensitizer depicted a promising future for cancer patients. This study evaluating on the radiosensitization effects of gold nanoparticles (AuNPs) for proton beam therapy using different radiobiological cell survival models. Human colon carcinoma cell lines (HCT 116) were used with 1.9 nm AuNPs and irradiated by different doses of a 150 MeV proton beam within the Spread-out Bragg Peak (SOBP) region. Clonogenic assay were used to obtain cell survival data which then be fitted to Linear Quadratic (LQ), Multi-target (MT), Repairable Conditionally Repairable (RCR), Pade' Linear Quadratic (PLQ), Kavanagh-Newman (KN), and Two Components (2C). The cellular uptake, localization, cytotoxicity and ROS measurement study were also conducted. The results show internalization of AuNPs manifested with the increase granulation of cells presented by side scattering (SSC) result of 7.3% compared to control. AuNPs were seen localized in the cytoplasm, yet no traces in nucleus area. Evaluation on the radiosensitization effects depicted sensitization enhancement ratio (SER) of 3.78 with LQ model, while other models also indicate similar increment of SER but less goodness of fit with the experimental data. The percentage of reactive oxygen species (ROS) induced by AuNPs are found to be around 234% which is double compared to control. In conclusion, the cell survival analysis with different radiobiological models shows radiosensitization effects by AuNPs when irradiated with proton beam. The evidence is also supported by the ROS data and the analysis of the model's parameter that could also be used to predict and quantify radiosensitization effects.

1. Introduction

Highly radio resistant tumours required accurate targeting and intense radiation dose to ensure effective treatment. Advanced modality such as proton beam therapy seems promising as proton relative biological effectiveness (RBE) is superior to photon therapy. Proton beam can yield free radicals within the Bragg peak area, giving off a sharp and high dose at particular depth (Belousov et al., 2020). Proton beam also produces dense ionization with high LET secondary particles localized at the tumor region, providing highly conformal dose distribution. The unique characteristic of a high-energy proton beam is that it delivers a superior optimal target precision and dose distribution compared to conventional photon beam radiotherapy (Durante & Flanz, 2019) Many clinical observations find that the proton beam therapy alone might be sufficient to treat tumours with very minimal dose to non-targeted normal tissues (Imaoka et al., 2019). Undeniably, new strategies are necessary to pursue better therapeutic efficiency.

Gold nanoparticles (AuNPs) have been widely investigated with

* Corresponding author. Centre for Diagnostic Nuclear Imaging, Universiti Putra Malaysia, 43400, Serdang, Selangor, Malaysia
E-mail addresses: raizulnasuha@upm.edu.my (R.A. Rashid), wnordiana@ukm.edu.my (W.N. Rahman).

https://doi.org/10.1016/j.jrras.2024.101203
Received 26 September 2024; Received in revised form 8 November 2024; Accepted 11 November 2024
Available online 29 November 2024

different modalities in radiotherapy. AuNPs have been proven to be an excellent radiosensitizer due to their high atomic number (Z), stable, generally inert, biocompatible and effective to reduce stenosis hemodynamic which is important characteristic as a drug in nanomedicine (Ali & Das, 2024; Kang et al., 2020; Waqas et al., 2023). An investigation combining 55 nm AuNPs with γ-ray from Cs-137 source showed excessive reactive oxygen species production with additional disruption of cytoskeletons and dysfunction of mitochondria when tested using laser scanning confocal microscopy (LSCM) (Tsai et al., 2022). Combination of PSMA-1-targeted Au_{25} nanoclusters with X-ray therapy are found to be effectively enhanced radiosensitization while having fast renal elimination that might simultaneously reduce the off-target effects and elemental toxicity (Luo et al., 2019). Various sizes and concentrations of AuNPs also could impact the image contrast quality (Harun et al., 2019). Other prospective radiosensitizers could include plant extracts (Sisin et al., 2021; Rahman et al., 2019) and other metallic nanoparticle such as bismuth oxide nanoparticles (Zainudin et al., 2020).

Several attempts have been documented on proton beam application with nanoparticles. The hypotheses of proton irradiation combined with nanoparticles (monometallic, bimetallic or trimetallic) gave higher cancer cell death than irradiation alone. In addition, studies generally showed that this combination treatment is selective for cancer cells and non-invasive to neighbouring normal cells (Klebowski et al., 2022). Previously, our team reported platinum and bismuth oxide nanoparticles as radiosensitizers irradiated with proton therapy, which showed the ability to influence reactive oxygen species (ROS) and cell deaths (Sisin, Rashid, et al., 2022; Anuar et al., 2021; Rashid et al., 2019). Besides proton therapy, bismuth oxide nanoparticles also had potential as radiosensitizers under photon beams, electron beams, and brachytherapy (Sisin et al., 2019, 2020; Zainudin et al., 2022). Dosimetric characterization of iron oxide nanoparticles and AuNPs with proton beam were evaluated and proven as prospective radiosensitizers (Sisin, Rashid, et al., 2022). The production of ROS aligned with the degree of radiosensitivity, with bismuth oxide nanoparticles showing the highest ROS levels, followed by platinum, AuNPs, and iron oxide nanoparticles (Anuar & Rahman, 2021). These nanoparticles could increase the radiation delivered in clinical proton beam settings (Rashid et al., 2019; Sisin, Rashid, et al., 2022). DNA dosimetry of the cancer cell in the presence of AuNPs irradiated by proton beams are found to give off high intensity of dose to cancerous cell at Bragg-peak area (Huynh & Chow, 2021). Evidence supported also by Belousov study that depicted the combination of AuNPs and proton may produce 5-fold increase in the dose at the edge of bragg-peak curve (Belousov et al., 2020). However, the enhancement's dependency remains unclear, where some study claimed that the actual behaviour may correlate to chemical and biological interactions (Klebowski et al., 2022; Shmatov, 2015; Cunningham et al., 2021).

Although several research have been done on proton beam therapy and AuNPs, the interaction mechanisms of dose enhancement or radiosensitization effects remain inconclusive. Many researches had applied standard Linear Quadratic model in various study translating dose conversion to clinical expectation, yet they also make comparison with other new and applicable models for more accuracy and verification, as the LQ model incapable to fit at high doses setting (Andisheh et al., 2013; Iwata et al., 2013; Brahme 2011; Ning et al., 1997). Moreover, a limited number of in vitro or in vivo studies manifest their outcome through radiobiological modelling comparison (Kempson, 2021; Andishsh et al., 2013; Lasalvia et al., 2019; Rashid, 2021). While understanding the underlying mechanisms is crucial, radiobiological modelling will provide a valuable reference for future clinical application development. The radiobiological models are use against the experimental data to emphasize the predicted mechanism that might happen at low and high doses responses. Meanwhile, Andisheh et al. had proven the beneficial of radiobiological modelling interpretation towards clinical application of the uncertainties in stereotactic high-dose radiotherapy at medium and low doses (Andisheh et al., 2013). Furthermore, a study have been conducted by comparing between LQ model and PLQ models on different dose fraction planning for malignant tumours radiotherapy treatment, for better cost-benefits and survival time outcomes (Lopes, 2022). Nevertheless, non-universally applicable model is still not found. Therefore for this study, those models are utilised to analyze the cell survival behaviour and to assess the validity of radiobiological models approach towards clinical setting on mechanism and technical interpretation at low and high doses outcome for combination treatment of proton beam with AuNPs.

In this paper, cell survival analysis of the radiosensitization effects by AuNPs under clinical proton beam irradiation is conducted. Several radiobiological models were employed against the cell survival experimental data which are; Linear Quadratic (LQ) as standard, Multi Target (MT), Repairable Conditionally Repairable (RCR), Pade's Linear Quadratic (PLQ), Kavanagh and Newman (KN), and Two-component (2C) models. This work also reported the cellular AuNPs uptake, localization, cytotoxicity, and reactive oxygen species (ROS) production AuNPs in combination with proton beam therapy.

2. Materials and methods

2.1. AuNPs preparation

The spherical shaped gold nanoparticles of 1.9 nm diameter were purchased from Nanoprobes Inc. (AuroVist® gold nanoparticle X-ray contrast agent; Yaphank, NY, USA). The gold nanoparticle was prepared by dissolving in Phosphate Buffered Saline (PBS) (Gibco, Life Technologies, CA, USA). The mixture was then sterilized using the centrifugal tube filter provided, then centrifuged at 10 000 g for 5 min. Finally, culture medium were used to dilute the solution to the required concentration.

2.2. Cell culture

The Human Colon Carcinoma (HCT 116) cell lines were cultured in McCoy's 5 A medium (Gibco, Life Technologies, UK), supplemented with 10% fetal bovine serum (FBS) (Gibco, Life Technologies, South America) and 1% antibiotics (10 000 units/mL penicillin and 10000 µg/ml streptomycin) (Gibco, Life Technologies, CA, USA). The cells were cultured and grown to confluence in a 75 cm^2 flask (Corning). The cells were incubated at the optimum condition of 37°C with 95% air and 5% CO_2 humidified atmosphere.

2.3. Cellular uptake measurement of AuNPs for HCT 116 cells

The study of cellular uptake of AuNPs was prepared by seeding 100 000 cells/well in 6 wells plates, left for 24 h, followed by adding 3 mMol/L of gold nanoparticles in each well. Then the incubation continued for the next 24 h. The next day, all the cells in each well were trypsinized by Trypsin-EDTA (0.25%) (Gibco, Life Technologies, CA, USA). Around 0.4 µL of cells suspension were collected and filled into 0.5 µL microcentrifuge tube. Propidium Iodide solution (Invitrogen, Thermo Fisher Scientific, California, USA) was added at final concentration of 10 µg/mL, about 30 min before running the flow cytometry.

2.4. AuNPs localization by light microscopy for HCT 116 cells

This study was conducted by seeding the 1000 cells per well into 6-well plates, with and without 1 mMol/L of 1.9 nm AuNPs. The plates were incubated for 24 h at 37°C and a 5% CO_2 humidified environment. After 24 h of incubation, the cells were washed twice with 1 ml of PBS and were fixed with 1 ml of ice-cold methanol for 15 min. After the fixation, the cells were stained with 0.5 % crystal violet in methanol for 15 min. Then the cells were washed gently with tap water until all the remaining crystal violet was cleared. The images of the cells were observed and captured using an Image Analyzer Microscope Olympus

Model: BX41/CVXS (Olympus Scientific Solutions Americas Inc, MA, USA) using magnification (100X) (Rashid et al., 2018). All samples were prepared in triplicate, and the study was repeated three times.

2.5. AuNPs cytotoxicity test

This study was conducted to determine the cytotoxicity effects (the degree to which an agent has specific destructive action on certain cells) of AuNPs without radiation exposure. The cells were seeded in 96 wells plates (1000 cells per well), and different concentrations of 1.9 nm AuNPs (1, 2, and 3 mMol/L) were used in this test. The cell viability was assessed after 24, 48 and 72 h of incubation with AuNPs. The test was performed using 10 µl of PrestoBlue® reagent (Fisher Scientific, London, UK) that was added to each sample and incubated at 37°C under 5% CO_2 for 2 h. After 2 h, the color of the PrestoBlue® reagent in the cell samples changed according to the number of viable cells. The optical density or absorbance of the reagent color that indicated the cell viability was measured using microplate reader model 680 (Bio-Rad Laboratories, CA, USA). The absorbance was read and recorded at 570 nm with a reference wavelength of 600 nm for normalization.

2.6. Cell irradiation procedure

The cells were prepared in suspension into a 0.5 ml microcentrifuge tube, with 1000 cells count/tube, then 1 mMol/L concentration of AuNPs as an optimal concentration was mixed directly into the cell's samples. Each treatment sample was prepared in triplicate and coupled with control samples (without AuNPs). All sample preparation was conducted at the Division of Radiation Oncology, Kobe University Graduate School of Medicine, Kobe City, Hyogo, Japan. The cell samples were placed on solid water phantom at a source-to-surface distance (SSD) of 100 cm using 6.5 × 20 cm^2 field sizes. , the plastic water phantoms were placed on the top as a build-up medium to ensure the samples received the maximum dose so that their position was within the Spread-Out Bragg Peak (SOBP) area. The energy of a 150 MeV proton beam was used for this irradiation. Irradiations were done in a single fraction with radiation doses ranging from 0 to 4 Gy. This proton experiment was conducted at Hyogo Ion Beam Medical Center, Tatsuno City, Japan.

2.7. Cell survival measurements

Clonogenic assays were carried out to obtain the survival curves, conveying the radiation effects quantitatively. All the protocols of clonogenic assay had been standardized and optimized, similar to the previous experimental work using conventional radiotherapy beams (Rashid et al., 2018). After irradiation, the irradiated samples were re-cultured and incubated for two weeks under the optimum condition in the cells' incubator. After the incubation period, the colonies of cells formed were fixed with ice-cold methanol, stained with crystal violet, and dried at room temperature. The image of a fixed single-cell colony was scanned using an Epson Expression 10 000 XL flatbed scanner (Seiko Epson Corp., Nagano, Japan) with a resolution of 300 DPI. The images were further analyzed using ImageJ software (version 1.41o, Java 1.6.0_10, Wayen Rasband, U.S. National Institutes of Health, Bethesda, MD, USA). Survival fractions were calculated and represented by the ratio of colony formation after exposure to radiation to the control colonies, which were unexposed to radiation.

2.8. Intracellular ROS measurements

ROS measurement was conducted to determine both physiological and pathological defects in the subcellular environment by detecting the amount of ROS such as superoxide and hydrogen peroxide that arise inside the irradiated cells. For this measurement, the HCt 116 cells were growmn and plated in 96 wells black plates (1 × 104 cells/well), then treated with 1 mMol/L concentration of gold nanoparticles for 24 h before irradiation. The 2′,7′-dichlorofluoresceindiacetate (DCFH-DA) (Sigma-Aldrich Pty. Ltd., St Louis, Mo, USA) was used to detect intracellular ROS generation at 2 h post-irradiation using a fluorescence microplate (Fluoroskan Ascent FL, Type 374, Thermo Labs System Inc., Philadelphia, PA 19102 United State) at 485 nm excitation and 538 nm emission.

2.9. Radiobiological model analysis and quantification of radiosensitization

This study used six radiobiological models to analyze the cell survival curves with and without AuNPs obtained for irradiation with proton beams. The LQ, MT, RCR, PLQ, KN, and 2C models are used. Each model was generated according to its standard equation and fit the experimental data point using OriginPro 9.0 software (OriginLab Corporation, Northampton, MA, USA). The equations and parameters for each radiobiological model were tabulated in Table 1.

2.10. Methodology for quantifying the radiobiological enhancement impact of AuNPs

SER was calculated by taking the ratio of the dose that produces x% of cell survival fraction for control cells to the dose that produces x% of cell survival fraction for cells treated with AuNPs [28]. The calculation was done at 50%, 70% and 90% of the cell survival fractions. The SER calculation is shown in Equation (7).

$$SER_{SF\%} = \frac{Dose\ at\ x\%\ cell\ SF\ of\ cells\ without\ AuNPs\ (D_{control})}{Dose\ at\ x\%\ cell\ SF\ of\ cells\ with\ AuNPs\ (D_{AuNPs})} \quad (7)$$

2.11. Statistical analysis

Each sample was tested in triplicate and data were expressed as mean ± standard deviation. Statistical analysis was performed with the OriginPro 9.2 software.

3. Results and discussion

3.1. Gold nanoparticles (AuNPs) cellular uptake into HCT 116 cells

Gold nanoparticles cellular uptake into the cells was presented in Fig. 1. The flow cytometry analysis shows the population are detected and counted at P3, which provided information by the side scatter (SSC) intensity on granularity intercellular represent cells incubated with AuNPs compared to the control sample (Wu et al., 2019). The SSC signal parameter measured the AuNPs internalization by HCT 116 cells. The SSC parameter is more sensitive than forward scatter (FSC) in detecting

Table 1
Radiobiological models equations with their parameters.

Model	Parameters	Equation	
Linear Quadratic (LQ) Model	α, β	$S = \exp^{-(\alpha D+\beta D2)}$	(1)
Multi-target (MT) Model	D, D_0, n	$S = 1 - \left(1 - exp^{(-D/Do)}\right)^n$	(2)
Repairable Conditionally Repairable (RCR) Model	a,b,c	$S_{RCR}(D) = e^{-aD} + bDe^{-cD}$	(3)
Pade' Linear Quadratic (PLQ) Model	α, β, γ	$\ln(S_F) = \frac{(-\alpha D - \beta D^2)}{(1-\gamma D)}$	(4)
Kavanagh and Newman (KN) Model	Ko, Ko_G	$\ln(S_F) = -K_O D(1 - \exp(-K_{OG}D))$	(5)
Two Components (2C) Model	α_1,αn, n	$SF = \exp(-\alpha_1 D)(1 - (1 - \exp(-\alpha_n D))^n)$	(6)

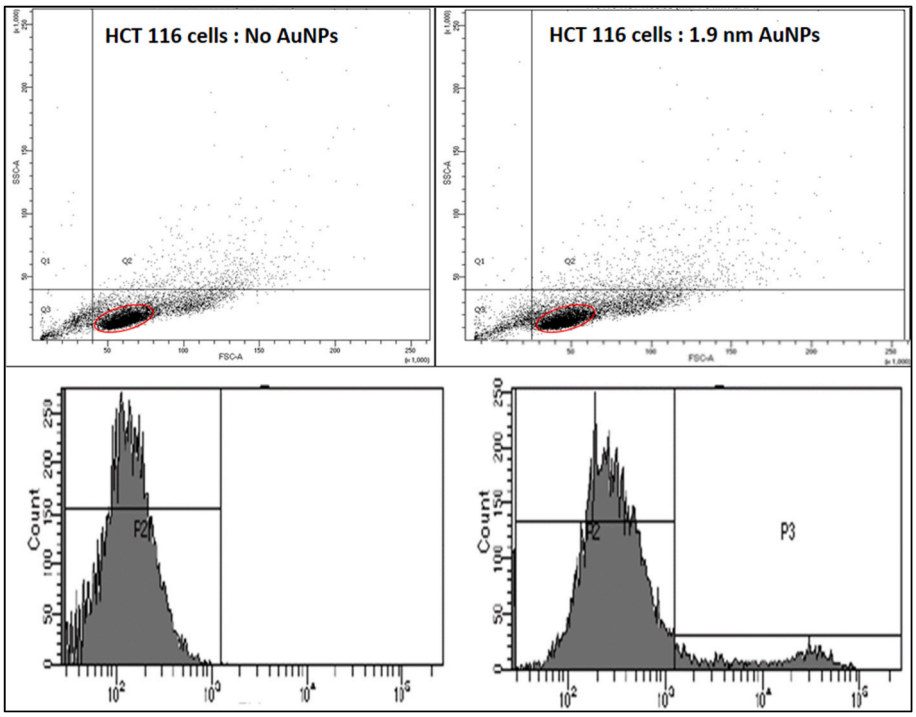

Fig. 1. The uptake of AuNPs into HCT 116 cells (a) No AuNPs (Control) and (b) 1.9 nm AuNPs.

small submicron particles, whether inside cells or in suspension (Toyooka T and Ibuki, 2012). In addition, it has been studied that the side scatters increase and forward scatter decreases upon the interaction of cells with laser light (Zucker et al., 2013). Moreover, AuNPs alone have high scattering detection which help analyze intracellular accumulation in cells (McQuaid et al., 2016).

3.2. Gold nanoparticles (AuNPs) localization for HCT 116 cells

Fig. 2 displays the light microscopy image of HCT 116 cells with AuNPs. AuNPs were observable in the cytoplasm of the cells. The internalization of AuNPs occurs through nanoparticle penetration at the cell surface membrane. The black traces of AuNPs were also found localized outside or on the nuclear envelope in the cluster form. In the middle of the cells where the nucleus is located, no traces of AuNPs were observed in the region, confirming that AuNPs cannot pass through nucleopores at cell's nuclear membrane.

This observation was in line with previous study by McQuaid and his colleagues, who found that localization of 1.9 nm AuNPs in MDA-MB-231 breast cancer cells was predominantly around the cytoplasmic area, which specifically accumulated close to nucleolus plasma (McQuaid et al., 2016). The AuNPs distribution is also found closely upon the nuclear membrane surrounding the inside and outside. The outcome concluded that no evidence of AuNPs was found within nuclei, yet most likely dispersed outside the nucleus (Cunningham et al., 2021). Evidence of numerous small spots found visible in cells co-cultured with 11-MUA coated gold nanoparticles (Zhang et al., 2021).

3.3. AuNPs cytotoxicity test on HCT 116 cells

The cytotoxicity results for 1.9 nm AuNPs on HCT 116 cells are shown in Fig. 3. The results indicate that 1.9 nm AuNPs induced minimal cytotoxicity on HCT 116 cells. The cell survival for 1 mMol/L of AuNPs

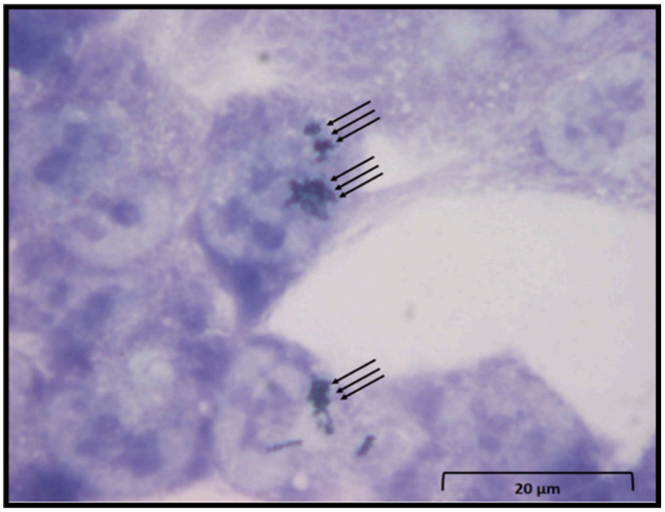

Fig. 2. AuNPs localization inside HCT 116 cells (100x magnifications).

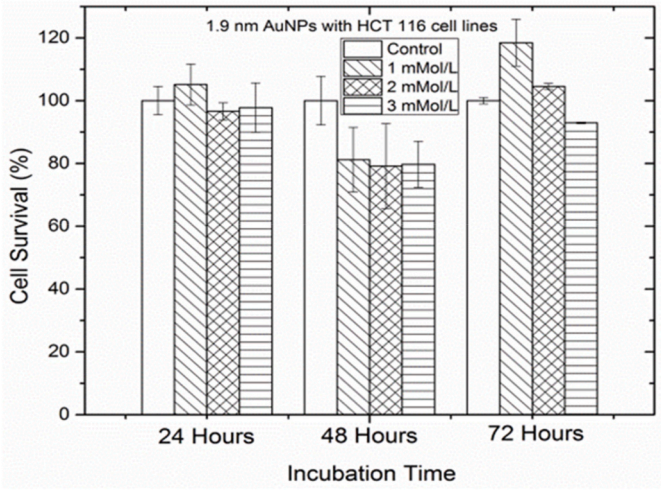

Fig. 3. The 1.9 nm AuNPs cytotoxicity on HCT 116 cells.

concentration is 105.11 % at 24 h, reduced to 81.14 % at 48 h, and back growing actively at 72 h with 118.47 % of cell survival. While at 2 mMol/L of AuNPs, the cell survival percentage was slightly higher at 24 h at 96.59 %, followed by a decrement to 79.19 % at 48 h and increased back to 104.54 % at 72 h incubation. The highest concentration of the AuNPs tested which is 3 mMol/L, depicted a slight decrement of cells survived at 24 h, around 97.77%. The treatment at 48 h impacted the cell survival with a decrement to 79.66 % of cells survival, and then at 72 h, the cell proliferation increased back to 92.94%.

3.4. Cell survival analysis using radiobiological models and quantification of sensitization enhancement ratio (SER)

Proton beam therapy has distinct characteristic as results from their interaction with medium. Radiobiological model especially LQ has been used widely for conventional photon beam to predict the biological response. This radiobiological model was tested for heavy particles treatment, especially with AuNPs (Franken et al., 2013). This study measured experimental cell survival data for 150 MeV proton beam from 0 to 4 Gy. The cells survival curves with and without AuNPs were generated by using radiobiological model; Linear Quadratic (LQ), Multi-Target (MT), Repairable Conditionally Repair (RCR), Pade Linear Quadratic (PLQ), 2 Component (2C) and Kavanagh and Newman (KN) model as shown in Fig. 4. The models have been fitted to the experimental data reasonably well except for KN model.

The comparison results for different radiobilogical model parameters were tabulated in Table 2. Application of the LQ model on the cell survival data shows acceptable curves with the R^2 value for control is 0.84 and AuNPs is 0.99. The cell survival curve with AuNPs depicted less cell survival than irradiation without AuNPs, indicating radiosensitization effects. LQ parameters result explained the increment at one hit due to one particle track (the linear component, α parameter) and two particles tracks (the quadratic component, β parameter), and additional with α/β ratio assumes the tumours radiobiological behaviour. The lethal damage to DNA strands may be irreparable with the increment of α and β parameters. The parameters forming the initial slope explained the survival curve and influenced the degree of downward curvature. Similar significant increment of α values instigated by 5-Fluorouracil antimetabolite in combination with bromodeoxyuridine or tantalum pentoxide nano-structured particles indicated more effective cell killings significantly impacts clinical application (McDonald et al., 2018). The Ctxb-AuNPs irradiation amplifies radiation-induced killing on A431 cells, showing α contribution of a lesion, which caused straight lethal cell damage (Li et al., 2019). According to previously published report, irradiation at 7% oxygenated cancer cells condition (close to normal human tissues) showed a more prominent β component that reflected the decrease in cells survival fraction at higher doses and increased oxygen conditions (greater cell-kills). Moreover, a test on cell irradiation under different O_2 conditions shows higher radiosensitive healthy cells given a lower 1.4 α/β ratio (McMullan et al., 2019). Therefore, the increment of the cell's sensitivity can be described with a big absolute value of β and a small absolute value of α/β towards this AuNPs radiosensitization.

The MT model shows better shoulder curvature and is well-fitted with AuNPs combination, especially at higher doses. The R^2 value for control sample is 0.55 and for AuNPs is 0.99. The MT model's parameters correlate with the intrinsic radiosensitivity with lower D and D_0 value. On the other hand, the parameter 'n' provides a higher value that explains contradicting mechanisms. Fertil and Malaise have proven a similar mechanismhat reflects the MT model's parameters relationship between the cells' radiosensitivity, which is indicated by the lower D and D_0 explaining the early effects of radiation (Fertil & Malaise, 1981). Other radiobiological analyses on radioimmunotherapy and external beam radiotherapy on human renal carcinoma xenografts survival had shown radiosensitivity of the Caki-1 tumor to the high dose rate and low dose rate treatments compared to the A498 tumor (Ning et al., 1997). Their parameters were represented with lower surviving fraction and quasi-threshold dose (Dq) (Ning et al., 1997). However, larger 'n' values demonstrated no correlation with the projected results by AuNPs as a radiosensitizer, even the cell survival curve presented had a steep initial slope. There are limited MT model applications in recent radiation biology studies.

Another radiobiological model approach used to emphasize the interaction of AuNPs as radiosensitizers is the RCR model. The RCR model might be able to interpret survival data very well, starting from the lowest doses, also called hypersensitive doses, transitional doses where the formation of survival curve's shoulder and at the end of the curve for highest doses. The RCR model's fitting curve showed

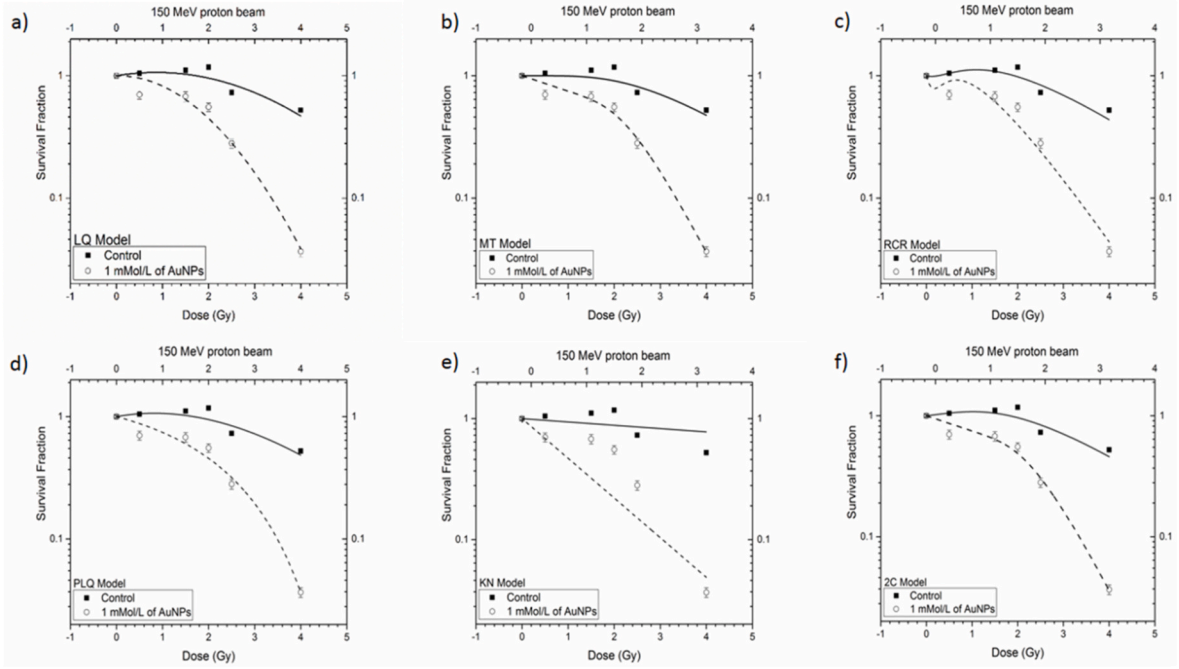

Fig. 4. The survival curves for 150 MeV proton beam fitted to different radiobiological models a) LQ, b) MT, c) RCR, d) PLQ, e) KN, f) 2C.

Table 2
Radiobiological parameters for LQ, MT, RCR, PLQ, KN and 2C models.

Proton Irradiation Setup (150 MeV)	Radiobiological Models and Parameters											
	Linear Quadratic (LQ) model				Multi-target (MT) model				Repairable Conditionally Repairable (RCR) model			
	Alpha (α)	Beta (β)	α/β ratio	R^2	D_1	D_0	n	R^2	a	b	c	R^2
Control	−0.15 ± 0.05	0.08 ±0.02	1.73	0.84	2.43[15] ± 0.00	1.69 ±1.55	6.56 ±12.26	0.55	2.39 ± 1.11	2.16 ±0.60	0.75 ±0.12	0.84
AuNPs	0.06 ± 0.15	0.19 ±0.04	0.32	0.99	3.46 ±1.49	0.72 ±0.11	32.45 ±33.89	0.99	6.95 ± 25.11	3.60 ±1.62	1.45 ±0.16	0.99
	Pade' linear quadratic (PLQ) model				Kavanagh and Newman (KN) model				Two-component (2C) model			
	α	β	γ	R^2	K_0	K_{0G}	R^2		α_1	α_n	n	R^2
Control	−0.16 ± 0.10	0.09 ±0.07	0.05 ±0.31	0.78	0.06 ±0.11	6.09[6] ±0.00	−2.16		−0.11 ±0.06	0.67 ±0.21	4.90 ±3.65	0.82
AuNPs	0.23 ±0.27	0.02 ±0.17	−0.16 ±0.13	0.99	0.76 ±0.58	688.52 ±0.00	−0.34		0.29 ±0.12	1.40 ±0.22	32.46 ±34.90	0.99

agreement with experimental data plotted with R^2 value for control is 0.84 and AuNPs is 0.99. The correlation results of the RCR model parameters show an increment of 'a' values of the initial mean number of damage events and 'b' values represent the maximum damage that happens but somehow may be repairable. In contrast, the last parameter of 'c' showed higher values, given the explanation of the mechanism of unrepairable damage caused by a complex complication. The RCR model may overcome the LQ model's limitation, enabling discussion on the wide range of dose effects individually.

On the other hand, PLQ model shows less fitting according to the R^2 value. The R^2 value for control is 0.78 and AuNPs is 0.99. However the survival curves by PLQ model provide a good AuNPs radiosensitization enhancement prediction. Further explanation of the PLQ parameters shows that the increment for the α and β values has proven the elevation of radiosensitivity intracellularly. At the same time, the decrement of γ explains the unrepairable lesions (Belkić & Belkić, 2013). PLQ model analysis was implemented to explain fractionated irradiation. The α (Gy-1), and β (Gy-2) components from the model described linear and quadratic effects that cause the DNA strand breakage. A clear result can be seen with the proton irradiation combined with AuNPs that shows increment for α and β values. However, PLQ and LQ models show correlation in treatments simulation, tested in a study to define the best treatment plan for malignant tumours (Belkić & Belkić, 2015).

Supporting evidence by the 2C model's parameters with fitting values (R^2; Control = 0.82, AuNPs = 0.99), revealing the increment of both α1 and αn, explained that the radiosensitization and dose enhancement increased with high values of the single hit at the early slope, plus multi-target at the final region of the dose curve. Andisheh and coworkers' study said that the 2C model could give better extrapolation at all data sets and explain the survival in the high dose region (Andisheh et al., 2013). The KN model's parameter also significantly increased with K_0 and K_g, representing an increment of quadratic mode and rate of potentially lethal lesions. However the goodness of fit showed lowest validation values (R^2; Control = −2.16, AuNPs = −0.34), In a nutshell, all model parameters visualized the effectiveness of AuNPs as a radiosensitizer especially for LQ and RCR models, except for KN models extrapolation, which considered null.

The quantification of the radiosensitization effects by AuNPs was conducted at different percentages of survival (50%, 70%, and 90 %) for all models. Table 3 shows that the SER increased at a higher percentage of survival (low dose range). The most prominent SER value with higher R^2 values can be seen with LQ and RCR models with 3.78 and 3.05 respectively. The same pattern showed by Cunningham and colleagues, describing higher SER values at 50% compared to 10% survival (Cunningham et al., 2021).

Table 3
The SER extrapolated from the cell survival curves generated from LQ, MT, RCR, PLQ and 2C models at 50, 70 and 90% survival.

Radiobiological Models	Sensitization Enhancement Ratio (SER)		
	50	70	90
LQ	2.18	2.52	3.78
MT	1.97	2.46	5.70
RCR	2.13	2.31	3.05
PLQ	2.13	2.68	5.47
2C	1.94	1.34	2.11

3.5. Reactive oxygen species (ROS) measurements

The radiosensitization effects are highly influences by the production of reactive oxygen species (ROS) that enhances the cell killing. Proton beam is a high LET radiation beam that is believed to cause ROS production, especially in the presence of AuNPs. Fig. 5 shows that combining AuNPs with proton irradiation resulted in potent ROS generation of up to 234%. It is estimated that around 70% of radiation-induced DNA damage is induced by indirect interaction. This interaction involved radiation energy imparted to the surrounding water produced free radicals and reactive oxygen species (ROS), the primary mediator that may cause radiolysis, attributed to DNA damage and cell death. The measurements of intracellular ROS or ROS in vitro solution have been performed by Baluchamy et al. to investigate the potential of ROS generation induced by proton beam (Baluchamy et al., 2010). According to a different study, 100 MeV proton beam might produce possible interactions of electron and x-ray beams emitted by Coulomb collision-driven with AuNPs (Anuar and Rahman, 2021, Sisin et al., 2022). This potent ROS production contributed to tumor dose

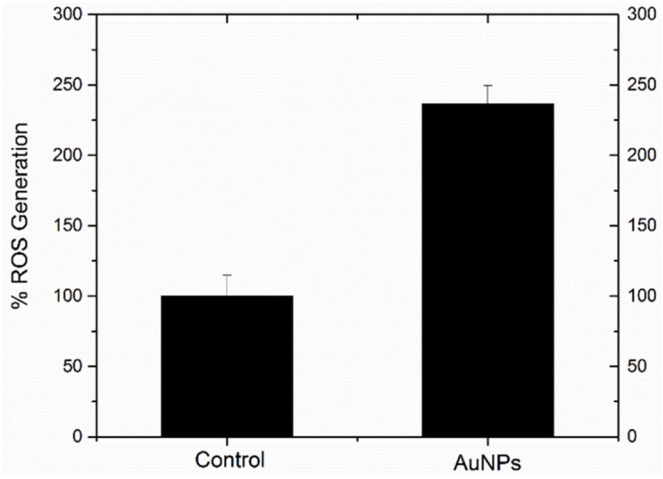

Fig. 5. The percentage of ROS production with and without 1.9 nm AuNPs after irradiation with 150 MeV proton beam at 2 Gy radiation dose.

enhancement or radiosensitization. Finding by Hespeels's study validated the interaction of proton and gold nanoparticles that induced dose enhancement by radiolysis mechanisms (Hespeels et al., 2019). Radiolysis significantly yielded inter-cluster absorption by enhanced destruction at nuclear membrane that caused potential holes permeable to oxidative species, thus maximizing biological DNA damage (Rajabpour et al., 2022).

4. Conclusions

Radiosensitization effects are observed for the AuNPs irradiated with proton beam therapy. Cell survival analysis using different radiobiological models visualized the effectiveness of AuNPs as a radiosensitizer, except for KN model. The model's parameter could be used to represent the possible physical, chemical and biological interactions that might occur during interaction of proton beams with AuNPs. The finding from ROS measurement also supports the results that correlate to the increase in radiosensitization effects with the increase in ROS production. Therefore, further study in precision of radiobiological characterization using specific models is important in order to elucidate the exact radiosensitization mechanisms by gold nanoparticles especially with proton beam. Improvement using mathematical models is required for treatment outcome prediction and hence upgrading overall effectiveness of cancer radiotherapy. In conclusion, this study gives the prediction on the effectiveness of proton beam and AuNPs as radiosensitizer, given agreement by the majority of the radiobiological model evaluated, thus technically depicted less dose of radiation needed to provide the same effects of damage.

CRediT authorship contribution statement

Raizulnasuha Ab Rashid: Writing – review & editing, Writing – original draft, Project administration, Methodology, Investigation, Formal analysis, Data curation. **Noor Nabilah Talik Sisin:** Writing – review & editing, Visualization, Validation. **Khairunisak Abdul Razak:** Resources. **Moshi Geso:** Validation, Supervision, Resources, Conceptualization. **Hiroaki Akasaka:** Methodology, Investigation, Conceptualization. **Ryohei Sasaki:** Methodology, Investigation. **Takahiro Tominaga:** Methodology, Investigation. **Hayato Miura:** Methodology, Investigation. **Masashi Nishi:** Methodology, Investigation. **Aml Aied Almutery:** Visualization, Validation. **Wan Nordiana Rahman:** Writing – review & editing, Supervision, Software, Resources, Project administration, Funding acquisition, Data curation, Conceptualization.

Acknowledgement

The authors express gratitude to Hyogo Ion Beam Medical Centre for providing their proton beam facilities for us to conduct this research. This project is supported by the Geran Galakan Penyelidik Muda Universiti Kebangsaan Malaysia (GGPM-2023-068).

References

Ali, A., & Das, S. (2024). Applications of neuro-computing and fractional calculus to blood streaming conveying modified trihybrid nanoparticles with interfacial nanolayer aspect inside a diseased ciliated artery under electroosmotic and Lorentz forces. *International Communications in Heat and Mass Transfer, 152*, Article 107313.

Andisheh, B., Edgren, M., Belkić, D., Mavroidis, P., Brahme, A., & Lind, B. K. (2013). A comparative analysis of radiobiological models for cell surviving fractions at high doses. *Technology in Cancer Research and Treatment, 12*(2), 183–192. https://doi.org/10.7785/tcrt.2012.500306

Anuar, M. A. K., & Rahman, W. N. W. N. (2021). Effect of nanoparticle size on radiosensitization effect and ROS generation in human colon carcinoma cells (HCT 116) after 150 MeV proton beam irradiation. *Journal of Nuclear and Related Technologies*, 17–25.

Baluchamy, S., Ravichandran, P., Periyakaruppan, A., Ramesh, V., Hall, J. C., Zhang, Y., … Ramesh, G. T. (2010). Induction of cell death through alteration of oxidants and antioxidants in lung epithelial cells exposed to high energy protons. *Journal of Biological Chemistry, 285*(32), 24769–24774. https://doi.org/10.1074/jbc.M110.138099

Belkić, D., & Belkić, K. (2013). Mechanistic repair-based Padé linear-quadratic model for cell response to radiation damage. *Advances in Quantum Chemistry, 65*, 407–449. https://doi.org/10.1016/B978-0-12-396455-7.00014-5. Academic Press.

Belkić, D., & Belkić, K. (2015). Mechanistic radiobiological models for repair of cellular radiation damage. *Advances in Quantum Chemistry, 70*, 163–263. Academic Press.

Belousov, A. V., Morozov, V. N., Krusanov, G. A., Moiseev, A. N., Davydov, A. S., Shtil, A. A., … Samoylov, A. S. (2020). The change in the linear energy transfer of a clinical proton beam in the presence of gold nanoparticles. *Biophysics, 65*(4), 541–547.

Cunningham, C., de Kock, M., Engelbrecht, M., Miles, X., Slabbert, J., & Vandevoorde, C. (2021). Radiosensitization effect of gold nanoparticles in proton therapy. *Frontiers in Public Health, 9*, Article 699822. https://doi.org/10.3389/fpubh.2021.699822

Durante, M., & Flanz, J. (2019). Charged particle beams to cure cancer: Strengths and challenges. , June *Seminars in Oncology, 46*(3), 219–225. WB Saunders.

Fertil, B., & Malaise, E. P. (1981). Inherent cellular radiosensitivity as a basic concept for human tumor radiotherapy. *International Journal of Radiation Oncology, Biology, Physics, 7*(5), 621–629.

Franken, N. A., Oei, A. L., Kok, H. P., Rodermond, H. M., Sminia, P., Crezee, J., … Barendsen, G. W. (2013). Cell survival and radiosensitisation: Modulation of the linear and quadratic parameters of the LQ model. *International Journal of Oncology, 42*(5), 1501–1515. https://doi.org/10.3892/ijo.2013.1857

Harun, A. Z., Ab Rashid, R., Ab Razak, K., Geso, M., & Rahman, W. N. W. A. (2019). Evaluation of contrast-noise ratio (CNR) in contrast enhanced CT images using different sizes of gold nanoparticles. *Materials Today Proceedings, 16*, 1757–1765. www.sciencedirect.comwww.materialstoday.com/proceedings2214-7853.

Hespeels, F., Heuskin, A. C., Tabarrant, T., Scifoni, E., Kraemer, M., Chêne, G., … Lucas, S. (2019). Backscattered electron emission after proton impact on gold nanoparticles with and without polymer shell coating. *Physics in Medicine and Biology, 64*(12), Article 125007. https://doi.org/10.1088/1361-6560/ab195f

Huynh, N. H., & Chow, J. C. (2021). DNA dosimetry with gold nanoparticle irradiated by proton beams: A Monte Carlo study on dose enhancement. *Applied Sciences, 11*(22), Article 10856. https://doi.org/10.3390/app112210856

Imaoka, T., Nishimura, M., Daino, K., Takabatake, M., Moriyama, H., Nishimura, Y., … Kakinuma, S. (2019). Risk of second cancer after ion beam radiotherapy: Insights from animal carcinogenesis studies. *International Journal of Radiation Biology, 95*(10), 1431–1440.

Iwata, H., Matsufuji, N., Toshito, T., Akagi, T., Otsuka, S., & Shibamoto, Y. (2013). Compatibility of the repairable-conditionally repairable, multi-target and linear-quadratic models in converting hypofractionated radiation doses to single doses. *Journal of Radiation Research, 54*(2), 367–373.

Kang, M. S., Lee, S. Y., Kim, K. S., & Han, D. W. (2020). State of the art biocompatible gold nanoparticles for cancer theragnosis. *Pharmaceutics, 12*(8), 701.

Kempson, I. (2021). Mechanisms of nanoparticle radiosensitization. *Wiley Interdisciplinary Reviews: Nanomedicine and Nanobiotechnology, 13*(1), Article e1656. https://doi.org/10.1002/wnan.1656

Klebowski, B., Stec, M., Depciuch, J., Panek, A., Krzempek, D., Komenda, W., … Parlinska-Wojtan, M. (2022). Improving the effect of cancer cells irradiation with X-rays and high-energy protons using bimetallic palladium-platinum nanoparticles with various nanostructures. *Cancers, 14*(23), 5899. https://doi.org/10.3390/cancers14235899

Lasalvia, M., Perna, G., Pisciotta, P., Cammarata, F. P., Manti, L., & Capozzi, V. (2019). Raman spectroscopy for the evaluation of the radiobiological sensitivity of normal human breast cells at different time points after irradiation by a clinical proton beam. *Analyst, 144*(6), 2097–2108. https://doi.org/10.1039/c8an02155d

Li, S., Bouchy, S., Penninckx, S., Marega, R., Fichera, O., Gallez, B., … Lucas, S. (2019). Antibody-functionalized gold nanoparticles as tumor-targeting radiosensitizers for proton therapy. *Nanomedicine, 14*(3), 317–333. https://doi.org/10.2217/nnm-2018-0161

Lopes, C. D. S. (2022). *Estudo Comparativo de Modelos radiobiológicos para Radioterapia na Modelagem Computactional de gliomas*.

Luo, D., Wang, X., Zeng, S., Ramamurthy, G., Burda, C., & Basilion, J. P. (2019). Targeted gold nanocluster-enhanced radiotherapy of prostate cancer. *Small, 15*(34), Article 1900968.

McDonald, M., Oktaria, S., Konstantinov, K., Rosenfeld, A., Lerch, M., Corde, S., & Tehei, M. (2018). Radiosensitisation enhancement effect of BrUdR and Ta2O5 NSPs in combination with 5-Fluorouracil antimetabolite in kilovoltage and megavoltage radiation. *Biomedical Physics & Engineering Express, 4*(3), Article 034001.

McMullan, T., Meehan, J., Langdon, S., McLaren, D., McLaughlin, S., & Nailon, B. (2019). Applying the linear quadratic model to PC-3 cells irradiated under different O2 conditions. April *Radiotherapy & Oncology, 133*. https://doi.org/10.1016/S0167-8140(19)32582-4. S1195-S1195). Elsevier House, Brookvale Plaza, East Park Shannon, Co, Clare, 00000, Ireland: Elsevier Ireland LTD.

McQuaid, H. N., Muir, M. F., Taggart, L. E., McMahon, S. J., Coulter, J. A., Hyland, W. B., … Currell, F. J. (2016). Imaging and radiation effects of gold nanoparticles in tumour cells. *Scientific Reports, 6*(1), Article 19442. https://doi.org/10.1038/srep19442

Ning, S., Trisler, K., Wessels, B. W., & Knox, S. J. (1997). Radiobiologic studies of radioimmunotherapy and external beam radiotherapy in vitro and in vivo in human renal cell carcinoma xenografts. *Cancer: Interdisciplinary International Journal of the American Cancer Society, 80*(S12), 2519–2528. https://doi.org/10.1002/(sici)1097-0142(19971215)80:12+<2519::aid-cncr26>3.3.co;2-t

Rahman, W. N., Mat, N. F. C., Long, N. A. C., Ab Rashid, R., Dollah, N., & Abdullah, R. (2019). Radiosensitizing effects of Oroxylum indicum extract in combination with megavoltage radiotherapy beams. *Materials Today: Proceedings, 16*, 2072–2077.

Rajabpour, S., Saberi, H., Rasouli, J., & Jabbari, N. (2022). Comparing Geant4 physics models for proton-induced dose deposition and radiolysis enhancement from a gold

nanoparticle. *Scientific Reports, 12*(1), 1779. https://doi.org/10.1038/s41598-022-05748-0

Rashid, R. A. (2021). *Radiobiological modelling of gold nanoparticles radiosensitization effects in advanced radiotherapy*. PhD Thesis. Universiti Sains Malaysia; 2021.

Rashid, R. A., Abidin, S. Z., Anuar, M. A. K., Tominaga, T., Akasaka, H., Sasaki, R., … Rahman, W. N. (2019). Radiosensitization effects and ROS generation by high Z metallic nanoparticles on human colon carcinoma cell (HCT116) irradiated under 150 MeV proton beam. *OpenNano, 4*, Article 100027. https://doi.org/10.1016/j.onano.2018.100027

Rashid, R. A., Razak, K. A., Geso, M., Abdullah, R., Dollah, N., & Rahman, W. N. (2018). Radiobiological characterization of the radiosensitization effects by gold nanoparticles for megavoltage clinical radiotherapy beams. *Bionanoscience, 8*, 713–722. https://doi.org/10.1007/s12668-018-0524-5

Shmatov, M. L. (2015). An expected increase in the efficiency of antiproton cancer therapy with the use of gold nanoparticles. *Physics in Medicine and Biology, 60*(20), Article N383. https://doi.org/10.1088/0031-9155/60/20/N383

Sisin, N. N. T., Abidin, S. Z., Yunus, M. A., Zin, H. M., Razak, K. A., & Rahman, W. N. (2019). Evaluation of bismuth oxide nanoparticles as radiosensitizer for megavoltage radiotherapy. *International Journal of Advanced Science, Engineering and Information Technology, 9*(4), 1434–1443. https://doi.org/10.2478/pjmpe-2022-0008

Sisin, N. N. T., Akasaka, H., Sasaki, R., Tominaga, T., Miura, H., Nishi, M., … Rahman, W. N. (2022). Effects of bismuth oxide nanoparticles, cisplatin and baicalein-rich fraction on ROS generation in proton beam irradiated human colon carcinoma cells. *Polish Journal of Medical Physics and Engineering, 28*(1), 30–36. https://doi.org/10.2478/pjmpe-2022-0004

Sisin, N. N. T., Azam, N. A., Rashid, R. A., Abdullah, R., Razak, K. A., Abidin, S. Z., & Rahman, W. N. (2020). Dose enhancement by bismuth oxide nanoparticles for HDR brachytherapy. , March *Journal of Physics: Conference Series, 1497*(1), Article 012002. https://doi.org/10.1088/1742-6596/1497/1/012002. IOP Publishing.

Sisin, N. N. T., Rashid, R. A., Abdullah, R., Razak, K. A., Geso, M., Akasaka, H., … Rahman, W. N. (2022). Gafchromic™ EBT3 Film measurements of dose enhancement effects by metallic nanoparticles for 192Ir brachytherapy, proton, photon and electron radiotherapy. *Radiation, 2*(1), 130–148. https://www.mdpi.com/1524432Toduka.

Toyooka T, Y., & Ibuki, Y. (2012). Flow cytometric evaluation of nanoparticles using side-scattered light and reactive oxygen species-mediated fluorescence–correlation with genotoxicity. *Environmental Science and Technology, 46*(14), 7629–7636. https://doi.org/10.1021/es300433x

Tsai, S. W., Lo, C. Y., Yu, S. Y., Chen, F. H., Huang, H. C., Wang, L. K., & Liaw, J. W. (2022). Gold nanoparticles enhancing generation of ROS for Cs-137 radiotherapy. *Nanoscale Research Letters, 17*(1), 123.

Waqas, H., Farooq, U., Hassan, A., Liu, D., Noreen, S., Makki, R., … Ali, M. R. (2023). Numerical and Computational simulation of blood flow on hybrid nanofluid with heat transfer through a stenotic artery: Silver and gold nanoparticles. *Results in Physics, 44*, Article 106152.

Wu, Y., Ali, M. R., Dansby, K., & El-Sayed, M. A. (2019). Improving the flow cytometry-based detection of the cellular uptake of gold nanoparticles. *Analytical Chemistry, 91*(22), 14261–14267. https://doi.org/10.1021/acs.analchem.9b02248

Zainudin, N. H. M., Ab Razak, K., Abidin, S. Z., Abdullah, R., & Rahman, W. N. (2020). Influence of bismuth oxide nanoparticles on bystander effects in MCF-7 and hFOB 1.19 cells under 10 MV photon beam irradiation. *Radiation Physics and Chemistry, 177*, Article 109143. https://doi.org/10.1016/j.radphyschem.2020.109143

Zainudin, N. H. M., Sisin, N. N. T., Ab Rashid, R., Jamil, A., Anuar, M. A. K., Razak, K. A., … Rahman, W. N. (2022). Cellular analysis on the radiation induced bystander effects due to bismuth oxide nanoparticles with 6 MV photon beam radiotherapy. *Journal of Radiation Research and Applied Sciences, 15*(3), 318–325. https://doi.org/10.1016/j.jrras.2022.08.003

Zhang, P., Yu, B., Jin, X., Zhao, T., Ye, F., Liu, X., … Li, Q. (2021). Therapeutic efficacy of carbon ion irradiation enhanced by 11-MUA-capped gold nanoparticles: An in vitro and in vivo study. *International Journal of Nanomedicine*, 4661–4674. https://doi.org/10.2147/IJN.S313678

Zucker, R. M., Daniel, K. M., Massaro, E. J., Karafas, S. J., Degn, L. L., & Boyes, W. K. (2013). Detection of silver nanoparticles in cells by flow cytometry using light scatter and far-red fluorescence. *Cytometry, Part A, 83*(10), 962–972. https://doi.org/10.1002/cyto.a.22342